Two-qubit Quantum Computing with Pulsed NMR

Leo Zhou
MIT Department of Physics
(Dated: April 14, 2013)

By manipulating the nuclear spins of hydrogen and carbon atoms in the chloroform molecule, we have implemented several quantum algorithms with two qubits. Quantum logic gates were realized through a combination of 90° rotations along transverse axes as well as natural time evolution. The Deutsch-Jozsa algorithm for one-bit boolean functions and Grover's algorithm for $N = 4$ are executed successfully. We observed a minimum fidelity of ∼65% (compared to ideal pure states) for CNOT gate and Deutsch-Jozsa algorithm. We also observed robust oscillatory behavior of Grover's algorithm up to ∼60 iterations for hydrogen spectra. The decay time constants of deterioration of output in Grover's algorithm were found to be on the order of spin-spin relaxation time, T_2.

I. INTRODUCTION

As early as 1982, Feynman[1] has realized the potential of quantum mechanical system to perform computational tasks beyond the capacity of classical computers. In 1992, Deutsch and Jozsa[2] gave one of the first examples of a quantum algorithm that performed a calculation exponetially faster than what is possible classically. In our experiment, we will examine the output of a CNOT gate, Deutsch-Jozsa algorithm, as well as Grover's algorithm, performed with pulsed NMR on the hydrogen and carbon nuclei in the chloroform molecule. We will also explore the extent to which spin-lattice (T_1) and spin-spin (T_2) relaxation processes in NMR affect our ability to implement quantum algorithms.

I.1. Qubits and density matrices

The quantum analogue of a classical bit is the qubit, which is simply a state in a two-level system, e.g. the nuclear spin of an atom. For a two-spin/qubit system, the Hamiltonian can be approximated as

$$H = \frac{2\pi\hbar J}{4}\sigma_z \otimes \sigma_z + \frac{\hbar P_{x1}(t)}{2}\sigma_x \otimes I + \frac{\hbar P_{y1}(t)}{2}\sigma_y \otimes I + \frac{\hbar P_{x2}(t)}{2} I \otimes \sigma_x + \frac{\hbar P_{y2}(t)}{2} I \otimes \sigma_x \quad (1)$$

where J is a first-order spin-spin coupling constant between the two qubits in Hz, and $P_{ij}(t)$ are classical controls that allow to affect the state of a single qubit. In our system, we will take the first (left) qubit to be the hydrogen nuclear spin, and the second (right) qubit to be the carbon nuclear spin.

An arbitrary two-qubit state can be written in the basis $|\psi\rangle = \alpha|00\rangle + \beta|01\rangle + \gamma|10\rangle + \kappa|11\rangle$, where $|0\rangle$, $|1\rangle$ are respectively the spin up and down state of the relevant qubit. For an ensemble of two-qubit states, however, this representation is no longer sufficient. Physicists then adopt the formalism of a density matrix[3], which is defined as $\rho \equiv \sum_i p_i |\psi_i\rangle \langle\psi_i|$ for an ensemble of states $|\psi_i\rangle$ each with probability p_i. When there are more than one nonzero p_i, the system is in a mixed state; otherwise, it is in a pure state. In this formalism, the expected value of an observable corresponding to $\hat{M}$ is then simply Tr $(\rho\hat{M})$.

While quantum computers often require the input state to be in a pure state (e.g. $\rho_{00} = |00\rangle\langle 00|$), the nuclear spin states at thermal equilibrium are not in pure states in a typical NMR-based setup, due to fact that $\hbar\omega \ll k_B T$ at room temperatures. In fact, the initial state of the two qubits in chloroform is approximately

$$\rho = \frac{e^{H/k_B T}}{\text{Tr } e^{H/k_B T}} \approx \frac{I}{4} + 10^{-4}\text{diag } (5, 3, -3, 5) \quad (2)$$

Nevertheless, we can extract the signal from only the ρ_{00} state through the technique of temporal labeling, which consists of performing two CNOT-like operations on the thermal state to cyclically permute the last three diagonal entries in the density matrix. Then if we apply our operations to the three states and sum the resulted signals, which are traceless observables such as σ_x and σ_y, we can effectively obtain a readout signal as if we are applying operations only to the pure state ρ_{00}.

I.2. Quantum gates

Quantum gates are essentially any unitary operations on a system of qubits. In general, a quantum gate corresponding to an unitary operation U sends a density matrix $\rho \to U\rho U^\dagger$. An common example of a quantum gate on two-qubit is the CNOT gate, which is

$$U_{\text{CNOT}} = \begin{pmatrix} 1 & 0 & 0 & 0 \\ 0 & 1 & 0 & 0 \\ 0 & 0 & 0 & 1 \\ 0 & 0 & 1 & 0 \end{pmatrix} \quad (3)$$

In our NMR system, we are able to perform 90° rotations of each of the spins along the $\pm x$- or $\pm y$- axis by sending appropriate RF pulses. This means we can straightforwardly implement a gate such as

$$R_{x1} = I \otimes R_x\left(\frac{\pi}{2}\right) = \frac{1}{\sqrt{2}} \begin{pmatrix} 1 & i & 0 & 0 \\ -i & 1 & 0 & 0 \\ 0 & 0 & 1 & -i \\ 0 & 0 & -i & 1 \end{pmatrix} \quad (4)$$

where $R_x(\theta) = e^{-i(\theta/2)\sigma_x}$. Note the subscript 1 in R_{x1} means doing nothing to the first qubit. We can also allow free time-evolution of the qubit, which for an appropriate time $T = \frac{1}{2J}$ gives the unitary operation

$$\tau = e^{-i(2\pi J/4)T\sigma_z\otimes\sigma_z} = e^{i\pi/4}\text{diag}\,(-i, 1, 1, -i) \qquad (5)$$

Note in general, we can ignore any overall phase[3]. As a result we can implement $U_{\text{CNOT}} \equiv R_{y1}^\dagger \tau R_{y1} R_{x1} R_{x2} R_{y2} R_{x2}^\dagger$, where $R_{y1}^\dagger$ means rotation by 90° along the $-y$-axis.

I.3. Deutsch-Jozsa algorithm

Any one-bit binary function $f_i : \{0,1\} \to \{0,1\}$ belongs to one of four possible classes, summarized in the following truth table

x	$f_1(x)$	$f_2(x)$	$f_3(x)$	$f_4(x)$
0	0	1	0	1
1	1	0	0	1

Consider the problem where you are asked to determine whether an unknown f_i is balanced (i.e. $f_i \in \{f_1, f_2\}$) or constant ($f_i \in \{f_3, f_4\}$). Classically, you have to make two queries of f_i in order to differentiate between the two cases. Using the Deutsch-Jozsa algorithm, however, you only need to make one query.

We first need to implement the quantum gate U_{fi} as the quantum version of f_i, which operates as

$$U_{fi}\,|x\rangle\,|y\rangle = |x\rangle\,|f_i(x) \oplus y\rangle \qquad (6)$$

where $\oplus$ means addition in modulo 2. The Deutsch-Jozsa algorithm is the application of $R_{y2}^\dagger R_{y1} U_{fi} R_{y2} R_{y1}^\dagger$ to the pure state ρ_{00}. Then if the function f_i is balanced, the output state would be ρ_{10}; if f_i is constant, the output would be ρ_{00}. This allows us to differentiate balanced and constant f_i with just one application of U_{fi}.

I.4. Grover's algorithm

Consider the problem where you are asked to locate a specific object in an unsorted list of size N. Classically, you would have to go through the list and check whether each entry is the object you're looking for; this will take $N/2$ queries on average, so the number of operations grows as $O(N)$. Using Grover's algorithm, however, this can be done in $O(\sqrt{N})$ operations, which for large N is much faster than what is classically possible.

To understand how Grover's algorithm works, we first formalize the problem by considering a function $f : \{0, \ldots, N-1\} \to \{0,1\}$ such that if the object is located at entry w, then $f(w) = 1$ but $f(a) = 0\ \forall a \neq w$. Now the problem is reduced to finding w.

Grover's algorithm uses n qubits where $N = 2^n$. If $N < 2^n$, we can simply expand the domain of f. Then we can represent the integers $0, \ldots, N-1$ in binary, which correspond to states of the qubits (e.g. $|2\rangle = |10\rangle$). Now, we can implement f in the form of a phase oracle, which is the unitary operator $O_w = 1 - |w\rangle\langle w|$. In addition, consider the state $|\psi\rangle = H^{\otimes n}\,|0\ldots0\rangle = \frac{1}{\sqrt{N}}\sum_a |a\rangle$, where H is the Hadamard transform. Grover's algorithm also requires the implementation of $U_\psi = 2\,|\psi\rangle\langle\psi| - 1$. Now, in the basis of $\{|w^\perp\rangle, |w\rangle\}$, where $|w^\perp\rangle = \frac{1}{\sqrt{N-1}}\sum_{a\neq w}|a\rangle$, we can write

$$U_\psi O_w = \begin{pmatrix} \cos\theta & -\sin\theta \\ \sin\theta & \cos\theta \end{pmatrix} \qquad (7)$$

where $\cos\theta = 1 - \frac{2}{N}$[4]. Note $|\psi\rangle \approx |w^\perp\rangle$ for large N. Then Grover's algorithm, at its k^{th} iteration, generates the output $|\psi_k\rangle = (U_\psi O_w)^k\,|\psi\rangle$. As evident in the graphical representation in Fig. 1, if $k\theta \approx \frac{\pi}{2} \Leftrightarrow k \approx \frac{\pi}{4}\sqrt{N}$, then $|\psi_k\rangle \approx |w\rangle$. Hence, Grover's algorithm only requires $O(\sqrt{N})$ queries of $f(a)$, compared to $O(N)$ classically.

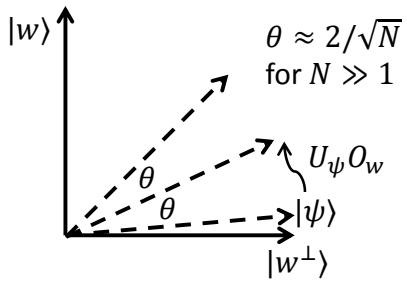

FIG. 1: Graphical representaion of Grover's algorithm.

Also evident in the graphical representation is the oscillatory behavior of Grover's algorithm's output. If we continue to apply the quantum gates $U_\psi O_w$, we will see for some k that $|\psi_k\rangle \approx -|w\rangle$, which will still give us the right answer since overall phase is ignored.

When $N = 4$, one iteration of Grover's algorithm will give us the exact desired answer as $U_\psi O_w\,|\psi\rangle = |w\rangle$. Since $\cos\theta = 1 - \frac{2}{4} = \cos 60^\circ$, the expected period of Grover's algorithm's oscillation is 3 iterations. We can implement Grover's algorithm for $N = 4$ with NMR, e.g.

$$U_\psi O_0 \equiv R_{x1} R_{y1} R_{x2} R_{y2} \tau R_{x1}^\dagger R_{y1}^\dagger R_{x2}^\dagger R_{y2}^\dagger \tau \qquad (8)$$

Similar expression can be obtained for $w = 1, 2, 3$. We can initialize the state $|\psi\rangle = H^{\otimes 2}\,|00\rangle$ with $H^{\otimes 2} \equiv R_{x1}^2 R_{y1} R_{x2}^2 R_{y2}$.

II. EXPERIMENTAL METHODS

Our experiment is conducted with a sample of chloroform ($^{13}CHCl_3$) through a special Bruker Avance 200 NMR spectrometer, which is controlled via a Linux workstation and with pulse programming and data acquisition

done in MATLAB scripts. As seen in Fig. 2, the spectrometer contains a large superconducting coil that generates a static magnetic field (B_0, in the z-axis by convention) in which protons have a Larmor frequency of approximately 200 MHz. The sample tube is mounted to a spinner and spun rapidly to average away any transverse inhomogeneities in B_0. The d6-acetone solvent contains deuterium, which produces a lock signal that is detected and used in a feedback loop to stabilize the axial magnetic field B_0[5].

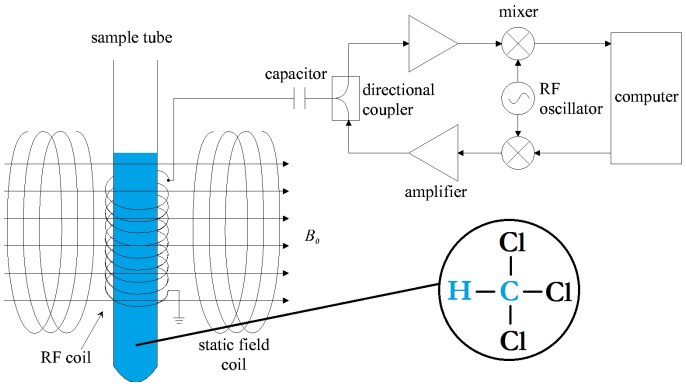

FIG. 2: The schematic diagram of our NMR spectrometer setup, adopted from Ref. [5]. A $^{13}CHCl_3$ (7% by weight) sample dissolved in d6-acetone is used.

A second coil oriented orthogonal to the main coil and wrapped around the sample tube is used to send RF pulses to the sample as well as detect the RF signal generated by the precessing nuclear spins. The programmable RF pulses, sent near their respective Larmor frequency, allow us to independently manipulate the nuclear spin states of both the hydrogen and carbon atom in the chloroform molecule. Depending on the relative phase in time we send the RF pulses, we can rotate the nuclear spin about $\pm x$- or $\pm y$-axis. The duration of the pulses allows us to set the angle of rotation.

A superheterodyne receiver allows us to differentiate the direction (clockwise/counterclockwise) of a spin's precession, and thus gives us a complex-valued voltage whose real and imaginary parts correspond to orthogonal components of the nuclear spin in the transverse plane.

Note we can probe the density matrix of the two-qubit system with their NMR spectra. Suppose the system is initially described by $\rho = \text{diag}\,(a, b, c, d)$, then we can apply a readout pulse R and measure the resulted FID signal. For example, $R = R_x(\frac{\pi}{2}) \otimes I$ for reading out hydrogen, and the readout voltage is mathematically given as $V_H(t) = -V_0 \text{Tr}\,(e^{-iHt} R\rho R^\dagger e^{iHt}[(i\sigma_x + \sigma_y) \otimes I])e^{-t/T_2}$. Applying one-sided Fourier transform, we can obtain the spectra in frequency domain for both qubits

$$\tilde{V}_H(f) = V_0\Big[\frac{a-c}{i(f+\frac{J}{2})+\frac{1}{2\pi T_2}} + \frac{b-d}{i(f-\frac{J}{2})+\frac{1}{2\pi T_2}}\Big] \quad (9)$$

$$\tilde{V}_C(f) = V_0\Big[\frac{a-b}{i(f+\frac{J}{2})+\frac{1}{2\pi T_2}} + \frac{c-d}{i(f-\frac{J}{2})+\frac{1}{2\pi T_2}}\Big] \quad (10)$$

They are the sums of two complex Lorentzian functions centered at $\pm J/2$, each with intensity proportional to some difference between two of the diagonal entries in the density matrix. If we assume that they are sufficiently far enough, we can consider the two Lorentzians independently. Now, for an individual complex Lorentzian,

$$\tilde{V}(f) = \frac{C}{if+\Gamma} = \frac{C\Gamma}{f^2+\Gamma^2} - i\frac{Cf}{f^2+\Gamma^2} = A - iD \quad (11)$$

where A is the absorptive spectrum, and D is the dispersive spectrum[6]. Ideally, we want to integrate just the absorptive A part, which normally would just be the real part, in order to recover the proportionality constant C. However, there may be a frequency dependent phase error $\phi(f)$ in a real system, so that our spectrum will be in the form of $\tilde{V}_{real}(f) = V(f)e^{i\phi(f)}$. To circumvent this problem, we instead integrate the power spectrum: $|\tilde{V}_{real}(f)|^2 = |\tilde{V}(f)|^2 = C^2/(f^2+\Gamma^2)$. Taking the square-root of the integral allows us to recover the magnitude of proportionality constant $|C|$. The sign of C can be obtained simply by inspecting the spectra.

III. DATA AND ANALYSIS

III.1. Calibration

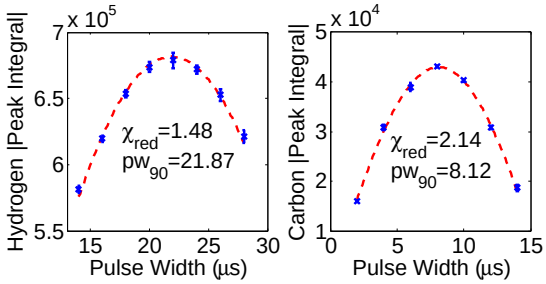

FIG. 3: Example calibration of 90° pulse width for both hydrogen and carbon, respectively.

We first determined the RF pulse widths corresponding to 90° rotation for hydrogen and carbon nuclear spins. Since a spin initially aligned with the z-axis will generate the maximal amplitude of precession signal when rotated 90°, we simply found the maximum of peak integrals when pulse width is varied from 1 to 30 μs by fitting them to a sinusoidal model, as seen in Fig. 3. This is performed in the beginning of every experiment session. Nevertheless, very little day-to-day variation is found. On average (over 9 days), $\text{pw}_{90}(H) = 22.74 \pm 0.20\mu$s, $\text{pw}_{90}(C) = 8.172 \pm 0.010\mu$s. The errors are standard statistical errors of the means.

We also estimated the spin-spin coupling constant J by looking at the peak separation in the NMR spectra of both hydrogen and carbon in the thermal state. This is also done every day when this constant is needed for proper execution of the unitary operation τ. On average (for 8 days), we found $J = 215.16 \pm 0.03(stat.)$ Hz.

III.2. Determination of Relaxation Constants

Using a 180°-t-90° pulse sequence, we were able to determine the spin-lattice relaxation time T_1, since the response should be proportional to $|2e^{-t/T_1} - 1|$, where t is the delay between the two pulses. We fitted |peak integral|, which corresponds to intensity of the response, against various t to the above model with an offset. Subsequently, we obtained estimates of T_1 for both hydrogen and carbon as $T_{1,H} = 18.66 \pm 0.28(stat.) \pm 0.60(syst.)$ sec and $T_{1,C} = 17.99 \pm 0.37(stat.) \pm 0.78(syst.)$ sec, where the statistical errors are from fitting, and systematic errors are estimated from the average deviation resulted from fitting only the left or only the right peaks. Since we set the delay between pulse sequence to be 100 sec $> 5T_1$, we expect that consecutive runs of pulse sequence did not significantly interfere with each other's results.

The spin-spin relaxation constant T_2, as evident from (9) and (10), is related to the width of the Lorentzian peaks in the NMR spectra. By fitting each of the two peaks of the thermal state spectrum as well as the left peak of ρ_{00} state spectrum to a Lorentzian function with an offset, we were able to obtain three estimates of each T_2 per day for 8 different days. Averaging them all, and taking the average difference of T_2 estimates from the two thermal state peaks as systematic error, we found $T_{2,H} = 0.067 \pm 0.005(stat.) \pm 0.005(syst.)$ sec and $T_{2,C} = 0.120 \pm 0.004(stat.) \pm 0.0001(syst.)$ sec.

III.3. CNOT gate and Deutsch-Jozsa algorithm

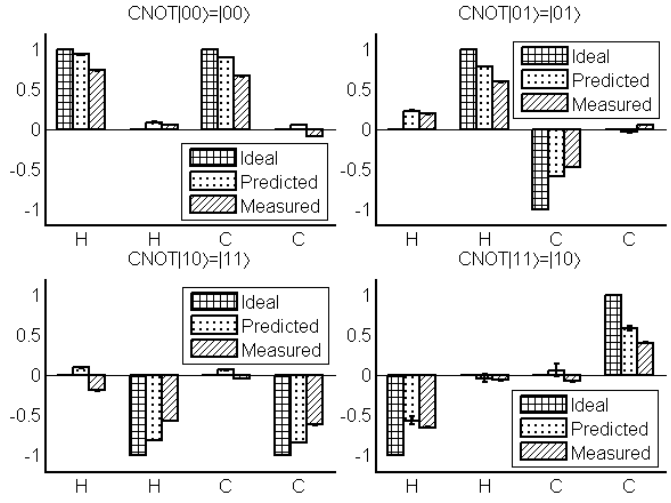

FIG. 4: CNOT gate output on the different basis states. Vertical axes are normalized peak integrals. Error bars are systematic due to varying integration regions.

Before every experiment, we obtained a spectrum for the supposed basis state ρ_{00} obtained from temporal labeling as a way to normalize our subsequent peak integrals, since ρ_{00} is supposed to have peak integral values corresponding to 1 and 0 for the left and right peaks in the spectra of both hydrogen and carbon. Since we don't expect our temporal labeling to be perfect, we normalize by the sum of the two peak integrals in each spectra. We also calculated the "true" density matrix of the initial state, which is close to but not exactly ρ_{00}, by converting the peak integral values $(a-c, b-d, a-b, c-d)$ to $\rho = \text{diag}\ (a, b, c, d)$. This way, we can propagate the initial state through our theoretical pulse sequences and obtain predicted outcomes for all our gates and algorithms. The results for CNOT are shown in Fig. 4, with systematic errors estimated as the difference from either integrating over a fixed region of frequency or a region obtained by fitting to Lorentzian. The results for Deutsch-Jozsa, while not shown, are very similar.

To quantitatively analyze how closely our measured outputs match our predictions, we adopt the concept of fidelity, which is defined as $F \equiv \langle\psi|\rho|\psi\rangle$ for a density matrix ρ supposedly representing a pure state $|\psi\rangle$. The computed results of both initial and final fidelities after applying either CNOT gate or Deutsch-Jozsa algorithm are shown in Table I. As we can see, our implementation produces results with minimum fidelity of ∼65% when evaluated for ideal pure state results, which are acceptable for most basic quantum computations.

CNOT gate				
	$00 \to 00$	$01 \to 01$	$10 \to 11$	$11 \to 10$
F_i	0.953 ± 0.005	0.799 ± 0.004	0.850 ± 0.001	0.690 ± 0.014
F_f	0.766 ± 0.004	0.672 ± 0.004	0.733 ± 0.003	0.644 ± 0.002
Deutsch-Jozsa algorithm				
	$DJ(f_1)$	$DJ(f_2)$	$DJ(f_3)$	$DJ(f_4)$
	$00 \to 10$	$00 \to 10$	$00 \to 00$	$00 \to 00$
F_i	0.953 ± 0.005	0.953 ± 0.005	0.953 ± 0.005	0.953 ± 0.005
F_f	0.808 ± 0.004	0.651 ± 0.003	0.866 ± 0.005	0.844 ± 0.004

TABLE I: Initial (F_i) and final (F_f) fidelities for CNOT gate and DJ algorithm. The errors are systematic, as statistical error are negligible in comparison.

III.4. Grover's algorithm

The spectra of both hydrogen and carbon, not shown here, exhibited the expected behavior of $U_\psi O_w H^{\otimes 2} |00\rangle = |w\rangle$ after one iteration of Grover's algorithm, with similar fidelities as CNOT and DJ. By plotting |normalized peak integral| against number of iterations (k) for Grover's algorithm, we observed an oscillatory behavior with period 3 as expected. An example for $w = 3$ case is shown in Fig. 5. First of all, notice there is very little difference between the peak integral values acquired for the same k but different days, evident in the region of k where there are overlapping data from different days. Also note that the hydrogen outputs seem more robust with a significant oscillation amplitude up to 60 iterations, whereas carbon's oscillations seem to flatten out at around 40 iterations. Also, hydrogen also has a consistently optimal peak integral every 3 iterations up

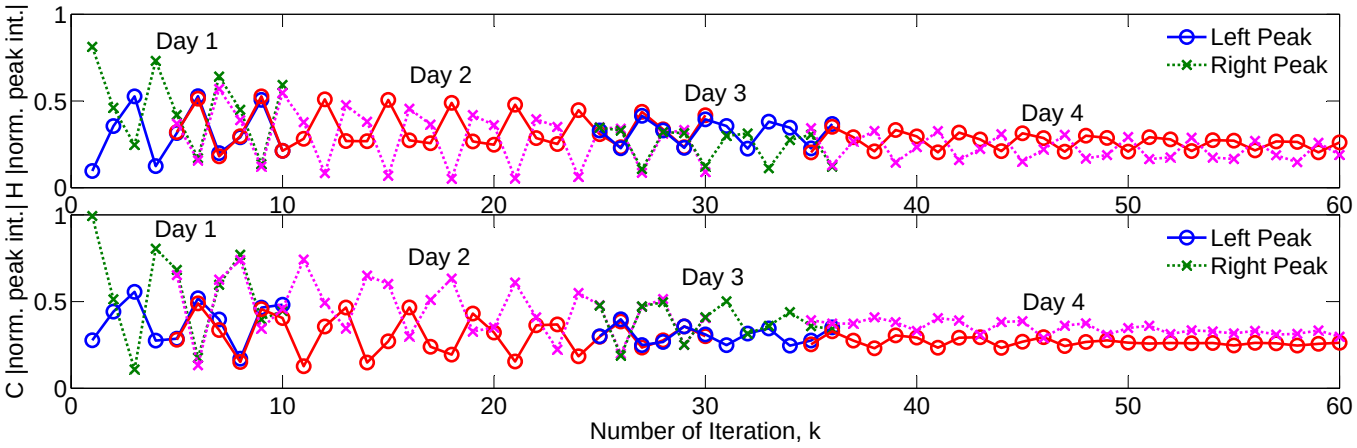

FIG. 5: Oscillatory behavior of Grover's algorithm output for $w = 3$ case. Top: hydrogen normalized peak integral. Bottom: carbon. The alternating colors are used to distinguish data acquired for different days.

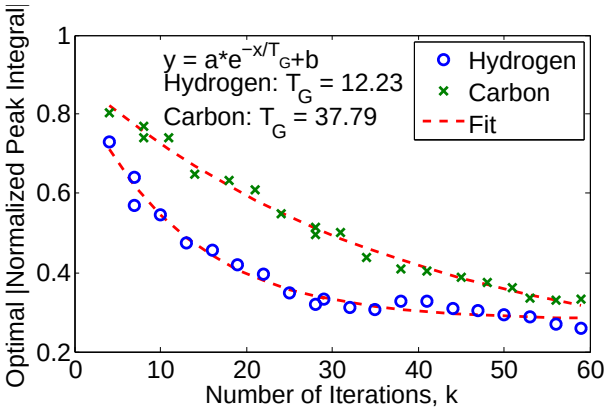

FIG. 6: An example of the decay of |peak integral| at optimal number of iteration k, for $w = 3$ case. T_G is in the units of number of iterations.

to 30 iterations, but carbon's optimal peak integrals start to occur "out of phase" as early as the 10^{th} iteration.

If we plot all the maxima of |normalized peak integral| against number of iteration k and examine its decay, as seen in Fig. 6, we can measure the decay constants of the deterioration of outputs in Grover's algorithm. Note each iteration takes approximately $1/J \approx 4.65$ ms due to the two τ operations, assuming each rotation operations take negligible time. Averaging the fit results for all w except for $w = 2$, whose fit result appeared to be an outlier, we obtained the following estimates for the decay constant of Grover's algorithm in units of time: $T_{G,H} = 0.057 \pm 0.0003(stat.) \pm 0.017(syst.)$ sec and $T_{G,C} = 0.157 \pm 0.038(stat.) \pm 0.039(syst.)$ sec. These correspond to about 12 and 34 iterations, respectively. The systematic errors are estimated from the average errors in the fitting procedures. Notice these values are close the T_2 estimates obtained earlier in §III.2.

IV. SUMMARY

We have successfully implemented two-qubit quantum computing with pulsed NMR on chloroform molecule, and performed CNOT gate operation, Deutsch-Jozsa algorithm as well as Grover's algorithm. For CNOT gate and Deutsch-Jozsa algorithm, we found that our implementation exhibited a minimum fidelity of approximately 65% when compared to ideal pure state results, which is acceptable for most basic quantum computations. Our Grover's algorithm implementation demonstrated robust oscillatory behavior up to 60 iterations, if one were to only to peek at the hydrogen spectra. We found that the decay constants for the output deterioration of Grover's algorithm are approximately $k = 12$ and 34 iterations for hydrogen and carbon respectively, which are on the order of their corresponding T_2 when converted into time units. This indicates that the spin-spin relaxation process is the most relevant source of decoherence in NMR-based quantum computers.

[1] R. Feynman, Int. J. Theor. Phys. **21**, 467 (1982).
[2] D. Deutsch and R. Jozsa, Proc. R. Soc. Lond. A **439**, 553 (1992).
[3] M. A. Nielsen and I. L. Chuang, *Quantum Computaion and Quantum Information* (Cambridge University Press, 2010).
[4] E. Farhi and S. Gutmann, Phys. Rev. A **57**, 2403 (1998).
[5] MIT Department of Physics, "Quantum Information Processing with NMR," (2010).
[6] G. Gemmecker, "Basic principles of FT NMR," (1999).